Phase Separation in Oxide−Borate Mixed Systems

D. Klimm,* R. Bertram, S. Ganschow, and J. Doerschel

Institute of Crystal Growth, Max-Born-Str. 2, 12489 Berlin, Germany

Single crystalline $GdCa_4O(BO_3)_3$ and $YCa_4O(BO_3)_3$ show one DTA melting peak at $t_f^{Gd} = 1490$ °C or $t_f^{Y} = 1504$ °C, respectively. Only pure $GdCa_4O(BO_3)_3$ and mixed crystals $Gd_{1-x}Y_xCa_4O(BO_3)_3$ with $x \lesssim 0.46$ showed one single peak also during cooling or during subsequent heating runs. The melting points of such intermediate compositions can be described well assuming ideal behavior of the solid as well as of the liquid phase resulting in a conventional quasibinary phase diagram with complete solubility and a narrow two-phase region solid/liquid. Compositions with $x \geq 0.5307$ show a miscibility gap in the liquid phase. For solidified pure $YCa_4O(BO_3)_3$ ($x = 1$), the content of the crucible was found to consist of the congruently melting compounds $Y_2Ca_3(BO_3)_4$, $Ca_3(BO_3)_2$, Y_2O_3 and of the original $YCa_4O(BO_3)_3$. The first three compounds built up a partial system of the concentration triangle B_2O_3, CaO, and Y_2O_3.

1. Introduction

Various RE (RE, rare earth element or yttrium) calcium oxyborates with the general formula $RECa_4O(BO_3)_3$ exhibit monoclinic acentric crystal symmetry. Norrestam et al.[1] reported the first X-ray diffraction measurements with small single crystals of the RE = La, Nd, Sm, Gd, Er, and Y compounds and discussed possible laser applications of this new substance class.

In the crystal structure,[2] calcium and gadolinium ions are surrounded by distorted oxygen octahedra. The $[REO_6]^{9-}$ octahedra built up chains along the crystallographic $\vec{c}$ axis, and the $[CaO_6]^{10-}$ octahedra form a 3-dimensional network. The different cation octahedra are partially sharing corners and are partially connected by triangular $[BO_3]^{3-}$ groups.

Single crystals of these materials combine (1) laser ion hosting (as almost all RE^{3+} ions can substitute each other in these materials) and (2) frequency doubling of laser radiation (because of the lack of a center of symmetry in the crystal structure). Nd:$GdCa_4O(BO_3)_3$, for example, shows under diode pumping at 810 nm laser action in the infrared at ≈1061 and ≈1091 nm simultaneously[3]. Because of the nonlinear properties of the $GdCa_4O(BO_3)_3$ matrix, it is possible to generate directly by self-frequency doubling green laser light at 530.5 nm. It is also possible to self-double another 936 nm emission of Nd:$GdCa_4O(BO_3)_3$, leading to blue laser emission, but only under pulsed titanium-sapphire laser pumping. However, a continuous wave blue laser beam is obtained in Nd:$GdCa_4O(BO_3)_3$ by self-sum-frequency mixing of the 1091 nm laser emission and the residual pump beam at 812 nm.

Large $YCa_4O(BO_3)_3$ crystals were grown and optically characterized by Iwai et al.[4] This substance has a much better temperature fluctuation acceptance than $GdCa_4O(BO_3)_3$, and 3rd harmonic generation of the 1064 nm emission of a Nd:YAG laser by type I phase matching is possible with $YCa_4O(BO_3)_3$ but not with $GdCa_4O(BO_3)_3$. Furuya et al. have successfully grown mixed crystals $Gd_{1-x}Y_xCa_4O(BO_3)_3$ with different composition x.[5] As the optical birefringence of such crystals depends on x, the noncritical phase matching wavelength for 2nd and 3rd harmonic generation could be adjusted by changing the yttrium concentration x. Inductively coupled plasma−optical emission spectrometry (ICP−OES) measurements of the gadolinium concentration ($1 - x$) along the growth axis of their crystals showed good homogeneity, indicating low segregation.

Irrespective of their importance for the development of a reproducible crystal growth technology, only few thermal properties (heat capacity and thermal expansion coefficients) of the $RECa_4O(BO_3)_3$ (RE = Gd, Y) crystals were measured so far.[2,6] Solid liquid-phase equilibria of the different rare earth calcium oxyborate systems were not yet published. The present paper reports on DTA measurements of mixtures between $GdCa_4O(BO_3)_3$ and $YCa_4O(BO_3)_3$. These results are compared with phase diagrams of other oxide-borate systems.

2. Experimental Section

The DTA measurements were performed with pieces of $GdCa_4O(BO_3)_3$ and $YCa_4O(BO_3)_3$ single crystals. Both crystals were grown by the Czochralski method from stoichiometric melts of dried Gd_2O_3 (or Y_2O_3, respectively), $CaCO_3$, and H_3BO_3 with 99.99% or 99.999% purity.[7] All growth experiments were performed under flowing nitrogen (99.999% purity) with a yield of ≈50% of the starting material. The successful growth of mixed crystals $Gd_{1-x}Y_xCa_4O(BO_3)_3$ was performed too, but these crystals were not used as starting material for the DTA measurements to avoid experimental error because of inaccurate concentration data of the solid phase. Instead, different mixtures of pure $GdCa_4O(BO_3)_3$ and $YCa_4O(BO_3)_3$ were used for thermal analysis.

The chemical element analysis of $Gd_{1-x}Y_xCa_4O(BO_3)_3$ with $0 \leq x \leq 1$ was carried out with parts from the shoulder (solidified first) and bottom (solidified last) of 5 Czochralski crystals using an inductively coupled plasma spectrometer Spectroflame-M (*Spectro Analytical Instruments, Germany*). This ICP−OES spectrometer was calibrated with simple synthetic standards. The precision is ≈3% RSD (relative standard deviation) for concentrations above BEC (background equivalent concentration). The results of the ICP−OES measurements are given in Table 1 and will be discussed in the next section.

* To whom correspondence should be addressed.

10.1021/je025574t CCC: $25.00
Published on Web 11/23/2002

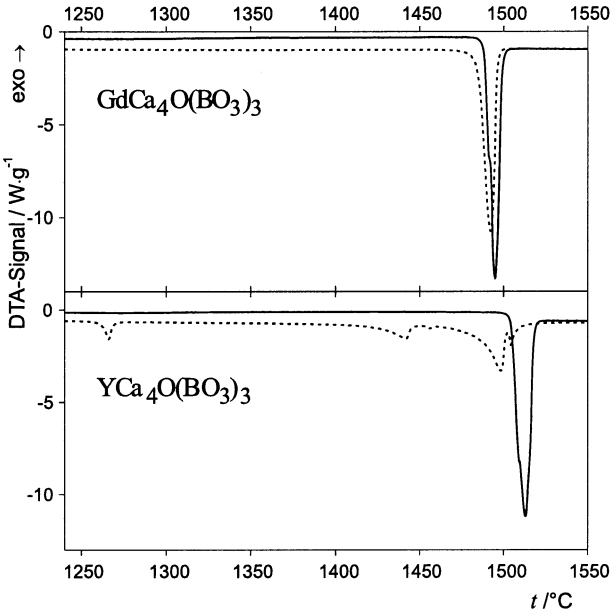

Figure 1. 1st heating (solid lines) and 2nd heating (dashed lines) of $GdCa_4O(BO_3)_3$ and $YCa_4O(BO_3)_3$ single crystals.

Table 1. ICP−OES Results of the Y Concentration x = [Y]/([Y] + [Gd]) of Different Parts of Czochralski Grown $Gd_{1-x}Y_xCa_4O(BO_3)_3$ Crystals

top (shoulder)	0.000	0.243	0.485	0.754	1.000
bottom	0.000	0.220	0.450	0.720	1.000

Simultaneous differential thermal analysis and thermogravimetry (DTA/TG) were performed with a NETZSCH STA 409C using a furnace with SiC heater and a HIGH RT 2 sample holder (Pt−Pt90Rh10 thermocouples). Calibration of the temperature t and sensitivity was performed at the melting points of Zn and Au and at the phase transitions of $BaCO_3$ with extrapolation to the higher t applied in the measurements with the oxyborates. The samples of typically 50 mg were placed in Pt95Au5 DTA crucibles with a lid. An empty crucible was used as reference. All samples were optically clear pieces of pure $GdCa_4O(BO_3)_3$ or $YCa_4O(BO_3)_3$ single crystals or mixtures of them. According to X-ray measurements, these samples did not contain any other phases. If not indicated otherwise, the measurements were performed in flowing air (50 mL/min) with the following program:

1. +10 K/min from 20 °C to 1560 °C
2. −10 K/min to 1000 °C
3. +10 K/min to 1560 °C
4. −10 K/min to 1000 °C
5. −30 K/min to 500 °C and stop.

3. Results

3.1. $GdCa_4O(BO_3)_3$ and $YCa_4O(BO_3)_3$. DTA curves for the 1st and 2nd heating cycle of pure $GdCa_4O(BO_3)_3$ and $YCa_4O(BO_3)_3$ are shown in Figure 1. The curves show for $GdCa_4O(BO_3)_3$ melting peaks at $t_f^{Gd} = 1490$ °C (1st heating) or 1485 °C (2nd heating). The small broadening and a shift to lower temperatures in the 2nd heating run can be attributed to different heat transfer from the crucible to the sample in the 2nd run. $YCa_4O(BO_3)_3$ shows in the 1st DTA heating run a sharp melting peak at $t_f^{Y} = 1504$ °C. The 2nd heating curve, however, shows as much as five endothermal peaks. As these peaks overlap partially, extrapolated onsets could not be found by the thermal analysis software. The peak minima of the dashed line in the lower part of Figure 1 are 1266 °C, 1442 °C, 1456 °C, 1498 °C, and 1504 °C. (The minimum of the $YCa_4O(BO_3)_3$ melting peak in the 1st run with an extrapolated onset of 1505 °C was 1513 °C.) From the area below the melting peaks, the heat of fusion could be estimated for both substances: $\Delta H_f^{Gd} \simeq 242$ kJ/mol and $\Delta H_f^{Y} \simeq 236$ kJ/mol. These values are expected to be accurate by ca. ±10%.

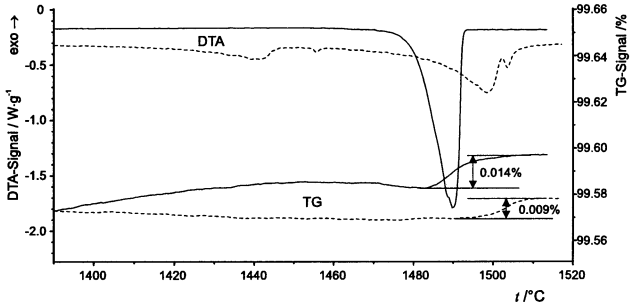

Figure 2. 2nd heating with 2 K/min of $GdCa_4O(BO_3)_3$ (full lines) and $YCa_4O(BO_3)_3$ (dashed lines).

After these DTA measurements, only the contents of the $GdCa_4O(BO_3)_3$ crucible, although polycrystalline, appeared optically clear. The contents of the $YCa_4O(BO_3)_3$ crucible instead were white but murky and contained submillimeter-sized slightly colored inclusions. To prove the estimated phase separation in $YCa_4O(BO_3)_3$ rich melts, additional DTA runs were performed. In these measurements, lower heating and cooling rates of only 2 K/min up to 1520 °C and an isothermal segment (5 h at 1520 °C) were used to allow maximum phase separation. The resulting DTA curves (Figure 2) were, regardless of the lower temperature change rate, very similar to the former ones (Figure 1) that were obtained at 10 K/min. However, a clear separation of the solidified melt into at least two phases could be observed much better after the DTA runs with ±2 K/min.

The melting process of both substances is accompanied by a reversible mass change of ≃0.01% (slightly more for the gadolinium compound and slightly less for the yttrium compound). One can assume that a minor change of the RE oxidation number is responsible for the TG step: The calculation of oxygen equilibrium fugacities at 1600 °C over the pure RE_2O_3 phases by the ChemSage computer program[8] gave $p_O^{Gd2O3} = 1.5 \times 10^{-10}$ bar and $p_O^{Y2O3} = 5.0 \times 10^{-12}$ bar, respectively. (O atoms have a higher fugacity than O_2 under such conditions.) If the mass change of 0.01% is completely attributed to the rare earth component of the oxyborates, it corresponds to a stoichiometry shift from $RE_2O_{2.994}$ to RE_2O_3. Obviously, the RE^{3+} are stable in the liquid phase and loose oxygen during coding. The reoxidation leads to a significant TG signal during melting that is shown in Figure 2.

No significant evaporation of the constituting oxides B_2O_3, CaO, and Y_2O_3, that should have lead to a permanent mass loss, could be observed during the DTA/TG measurements.

Figure 3 shows the contents of the DTA crucibles after the measurements with ± 2 K/min heating rate. The $GdCa_4O(BO_3)_3$ melt formed an optically clear polycrystalline body, but the $YCa_4O(BO_3)_3$ melt showed some regions of a clear and slightly orange/brownish phase (darker in the figure) surrounded by an opaque white mixture of different phases.

The $YCa_4O(BO_3)_3$ crucible in Figure 3 was cut, and the chemical composition of the different phases was measured by EDX. It was found that the orange/brownish phase is

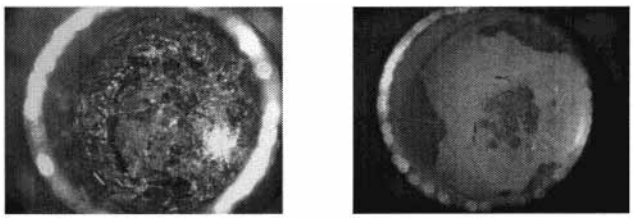

Figure 3. $GdCa_4O(BO_3)_3$ (left) and $YCa_4O(BO_3)_3$ (right) sample after DTA measurements. Diameter of the crucibles: 6.5 mm.

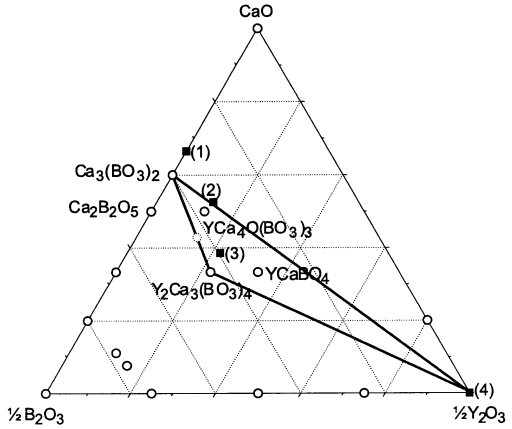

Figure 4. Phases in the systems $Re_2O_3-CaO-B_2O_3$ reported in the literature [Diagram nr. 234],[10−12] ○, and EDX results of phases found in this study in a slowly cooled $YCa_4O(BO_3)_3$ melt, ■.

almost pure Y_2O_3. No other chemical elements than Y and O contributed to the X-ray spectrum above the experimental scatter. The unexpected coloration of Y_2O_3 is expected to result from the incorporation of doping-level concentrations of Ca into the usually colorless Y_2O_3 matrix.[9] For phases within the opaque white main body of the melt, three different chemical compositions were found that are marked in Figure 4 by the filled squares (1)...(3), and Y_2O_3 is composition (4). Phases that are known to be stable in the ternary system $Y_2O_3-CaO-B_2O_3$ are marked by empty circles. The dashed circle between $Ca_3(BO_3)_2$ and $Y_2Ca_3(BO_3)_4$ corresponds to $YSr_3(BO_3)_3$ that is known to exist in the analogous ternary system $Y_2O_3-SrO-B_2O_3$. This compound melts congruently at 1400 °C[13] and Sr can at least partially be substituted by Ca. It is unknown whether the pure Ca compound $YCa_3(BO_3)_3$ exists.

The correspondence of the measured composition (4) to Y_2O_3 is obvious. The other compositions are interpreted as (1) ≙ $Ca_3(BO_3)_2$, (2) ≙ $YCa_4O(BO_3)_3$, and (3) ≙ $Y_2Ca_3(BO_3)_4$. All measured compositions (filled squares) are shifted toward lower boron contents [B] from the theoretical values for these three phases. This systematic error can be explained by the circumstance, that the content of the light element boron [B] can be obtained by EDX only indirectly via the determination of [Y], [Ca], and [O]. Therefore, the experimental errors are expected to be high.

3.2. Mixed Crystals $Gd_{1-x}Y_xCa_4O(BO_3)_3$. As already shown in Figure 1, $GdCa_4O(BO_3)_3$ as well as $YCa_4O(BO_3)_3$ show one sharp melting peak in the 1st DTA heating run. $GdCa_4O(BO_3)_3$ shows one single melting peak also in the 2nd and later heating runs. If small amounts (up to $x = 0.4615$) of $YCa_4O(BO_3)_3$ are mixed to $GdCa_4O(BO_3)_3$ in a 1st "melt together" run, the mixture shows during a 2nd heating one single melting peak as observed for $x = 0$ but with slightly increased t_f (Figure 5). The rise of t_f with x as well as the fraction of $YCa_4O(BO_3)_3$ in the solid phase (solidified first during crystal growth experiments) and in the liquid phase (≈ substance crystallized last in growth experiments, cf. Table 1) can be described assuming ideal mixing of liquid and solid phase. The two-phase region liquid/solid of the $x-t$ phase diagram $GdCa_4O(BO_3)_3-YCa_4O(BO_3)_3$ is narrow ($\Delta t_{max} < 1$ K and $\Delta x_{max} < 0.05$ for $x = 0.5$; Figure 2.[7]

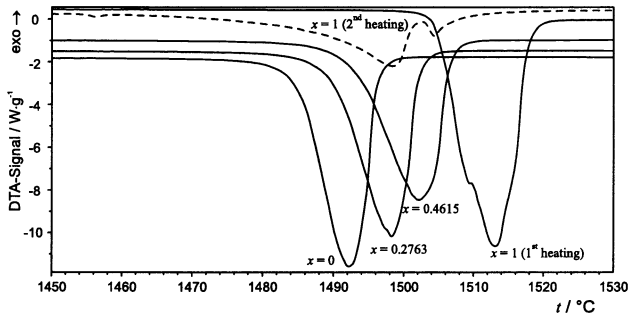

Figure 5. 2nd heating curves of $Gd_{1-x}Y_xCa_4O(BO_3)_3$ ($x = 0$, 0.2763, 0.4615) compared with the 1st heating curve of pure $YCa_4O(BO_3)_3$ ($x = 1$) and the 2nd heating curve of pure $YCa_4O(BO_3)_3$ (dashed line).

For higher concentrations of $YCa_4O(BO_3)_3$ (starting from $x = 0.5307$), a variety of DTA peaks and phase separation were found in the 2nd heating runs, similar as for pure $YCa_4O(BO_3)_3$ with $x = 1$.

4. Discussion

The congruently melting crystalline phases $Ca_3(BO_3)_2$, $Y_2Ca_3(BO_3)_4$, and Y_2O_3 built up a partial triangle within the ternary system $Y_2O_3-CaO-B_2O_3$ and are therefore found after slow cooling of the $YCa_4O(BO_3)_3$ crucible. The congruent melting behavior of $Y_2Ca_3(BO_3)_4$ was confirmed by additional DTA measurements of powder mixtures close to this composition. A melting temperature $t_f \approx 1340$ °C and comparably low $\Delta H_f \approx 150$ kJ/mol were estimated from these DTA data.

A crystallization process that starts within the partial triangle, whose borders are shown in Figure 4 by solid lines, cannot leave it. Therefore, only phases within this smaller system are important for a discussion of the crystallization process. $YCaBO_4$ within the partial system was found by subsolidus annealing experiments[10] and as a white powder on the surface of Czochralski grown $Y_2Ca_3(BO_3)_4$ crystals.[13] It could not be observed during our measurements.

$YCa_4O(BO_3)_3$ decomposes during melting in two liquids with different composition. If the subsequent cooling is performed in a suitable manner, the decomposition is reversible and $YCa_4O(BO_3)_3$ is formed again in a monotectic reaction. Such behavior can be obtained during crystal growth processes. During very slow cooling processes and without stirring, the two liquids remain unmixed and cool separately. $Ca_3(BO_3)_2$, $Y_2Ca_3(BO_3)_4$, Y_2O_3, and $YCa_4O(BO_3)_3$ are the products of this cooling process. The remelting of this mixture of four crystalline phases leads to a variety of melting peaks during the 2nd DTA run of $YCa_4O(BO_3)_3$ (Figure 1).

In contrast to $YCa_4O(BO_3)_3$, $GdCa_4O(BO_3)_3$ does not separate in two liquids during the melting process. Therefore, the melting process is always completely reversible. Mixed crystals $Gd_{1-x}Y_xCa_4O(BO_3)_3$ can be obtained for all compositions $0 \le x \le 1$, as no miscibility gap exists in the solid phase. Because of the narrow two-phase region liquid/solid in the pseudobinary phase diagram, the segregation during the crystallization of mixed crystals is small, and a crystal with homogeneous composition along the growth

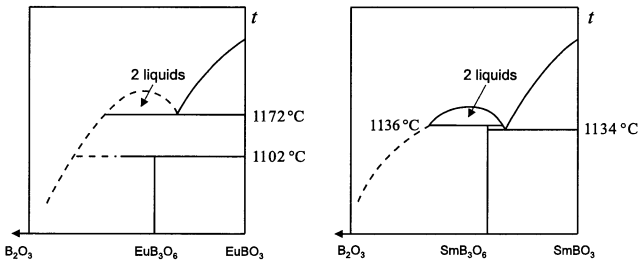

Figure 6. Phase diagrams B_2O_3−$REBO_3$ for RE = Eu ($r_{Eu^{3+}}$ = 108.7 nm) and RE = Sm ($r_{Sm^{3+}}$ = 109.8 nm) [Diagrams nr. 4383 + 4388].[11]

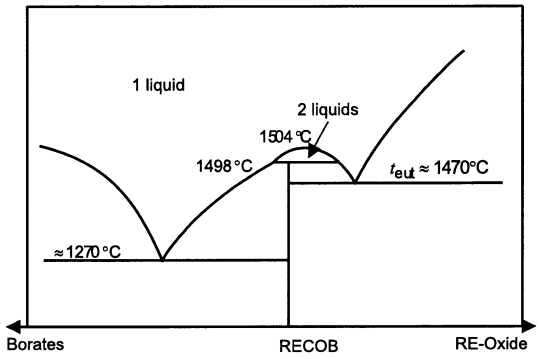

Figure 7. Proposed scheme for a binary section of Figure 4 that crosses the RE oxyborate composition. Temperatures given here are valid for RE = Y.

axis can be obtained. The crystal with the highest $YCa_4O(BO_3)_3$ concentration that showed completely reversible congruent melting was $x = 0.4615$.

The behavior of the different ternary systems $Ca_3(BO_3)_2$−$RE_2Ca_3(BO_3)_4$−RE_2O_3 can be compared with the well-known binary systems B_2O_3−$REBO_3$ (Figure 6). These systems show a miscibility gap in the liquid phase between $REBO_3$ and B_2O_3. The lowest temperature, where two liquid phases can be observed (t_{eut} close to $REBO_3$), drops considerably and almost linearly with increasing radius of the RE^{3+} ion and ranges from 1473 °C for luthetium to 1172 °C for europium. Starting from gadolinium, with increasing RE^{3+} ions, an intermediate compound REB_3O_6 becomes more and more stable. NdB_3O_6 shows already congruent melting at 1155 °C [Diagram 4387].[11] SmB_3O_6, however, decomposes at 1136 °C in an oxide-rich and in a borate-rich (B_2O_3) melt. Such peritectic decomposition is also shown by $YCa_4O(BO_3)_3$. As for the REB_3O_6, the stability of the $RECa_4O(BO_3)_3$ increases with $r_{RE^{3+}}$ and the melting behavior changes from incongruently for the yttrium compound ($r_{Y^{3+}}$ = 104.0 nm) to congruently for gadolinium ($r_{Gd^{3+}}$ = 107.8 nm). The turnover for mixed crystals was observed close to $x = 0.5$; this corresponds to an average ion radius ($r_{Y^{3+}} + r_{Gd^{3+}}$)/2 = 105.9 pm (between terbium and dysprosium). For smaller RE^{3+}, the "2 liquid" region is expected to appear, and for larger RE^{3+} (starting from Tb^{3+}), it is not.

Figure 7 shows a schematic binary section through the ternary system crossing the rare earth oxyborate composition $RECa_4O(BO_3)_3$. Like for SmB_3O_6, the decomposition (during the melting process) of $YCa_4O(BO_3)_3$ in two different liquids is assumed. This decomposition corresponds to the single melt peak of pure $YCa_4O(BO_3)_3$ at 1505 °C (Figure 1). During cooling in the DTA run, from these liquids crystallizes $YCa_4O(BO_3)_3$ and later (after reaching the eutectic temperatures on both sides) Y_2O_3 or $Ca_3(BO_3)_2$ and $Y_2Ca_3(BO_3)_4$, respectively. All of these four phases were found by EDX analysis (Figure 4). During the 2nd DTA run, the different eutectics melt separately giving rise to a variety of DTA peaks. The highest peak coincides with the single peak of the 1st heating run, as the melting of the first precipitate $YCa_4O(BO_3)_3$ proceeds at the same temperature 1504 °C.

Acknowledgment

$GdCa_4O(BO_3)_3$ single crystals were grown by A. Kłos (Institute of Electronic Materials Technology, Warsaw). K. Petermann (University Hamburg) and A. Pajączkowska (Institute of Electronic Materials Technology, Warsaw) are acknowledged for fruitful hints and discussion. The authors are indebted to V. Bermúdez (Universidad Autónoma de Madrid) for cooperation.

Literature Cited

(1) Norrestam, R.; Nygren, M.; Bovin, J. O. Structural Investigations of New Calcium−Rare Earth (R) Oxyborates With the Composition $Ca_4RO(BO_3)_3$. *Chem. Mater.* **1992**, *4*, 737−743.
(2) Mougel, F.; Kahn-Harari, A.; Aka, G.; Pelenc, D. Structural and thermal stability of Czochralski grown GdCOB oxoborate single crystals. *J. Mater. Chem.* **1998**, *8*, 1619−1623.
(3) Vivien, D.; Mougel, F.; Auge, F.; Aka, G.; Kahn-Harari, A.; Balembois, F.; Lucas-Leclin, G.; Georges, P.; Brun, A.; Aschehoug, P.; Benitez, J.-M.; Le Nain, N.; Jacquet, M. Nd:GdCOB: Overview of its Infrared, Green and Blue Laser Performances. *Opt. Mater.* **2001**, *16*, 213−220.
(4) Iwai, M.; Kobayashi T.; Furuya, H.; Mori, Y.; Sasaki, T. Crystal Growth and Optical Characterization of Rare-Earth (Re) Calcium Oxyborate $ReCa_4O(BO_3)_3$ (Re = Y or Gd) as New Nonlinear Optical Material. *Jpn. J. Appl. Phys.* **1997**, *36*, L276-L279.
(5) Furuya, H.; Yoshimura, M.; Kobayashi, T.; Murase, K.; Mori, Y.; Sasaki, T. Crystal Growth and Characterization of $Gd_xY_{1-x}Ca_4O(BO_3)_3$ Crystal. *J. Crystal Growth* **1999**, *198/199*, 560−563.
(6) Wang, C.; Zhang, H.; Meng, X.; Zhu, L.; Chow, Y. T.; Liu, X.; Cheng, R.; Yang, Z.; Zhang, S.; Sun, L. Thermal, Spectroscopic Properties and Laser Performance at 1.06 and 1.33 μm of Nd: $Ca_4YO(BO_3)_3$ and Nd: $Ca_4GdO(BO_3)_3$ Crystals. *J. Cryst. Growth* **2000**, *220*, 114−120.
(7) Klimm, D.; Ganschow, S.; Bertram, R.; Doerschel, J.; Bermúdez, V.; Kłos, A. Phase Separation During the Melting of Oxide Borates $LnCa_4O(BO_3)_3$ (Ln = Y, Gd). *Mater. Res. Bull.* **2002**, *37*, 1737−1747.
(8) PC Code "ChemSage" and "SPS96TO2 - SGTE Pure Substance Database". GTT Technologies, Kaiserstr. 100, D-52134 Herzogenrath, Germany. http://gttserv.lth.rwth-aachen.de/∼sp/tt/.
(9) Petermann, K. Private communication 2002.
(10) Zhang, Y.; Chen, X. L.; Liang, J. K.; Xu, T.; Xu, Y. P. Phase Relations in the System Y_2O_3-CaO−B_2O_3. *J. Alloys Compd.* **2001**, *327*, 132−135.
(11) Levin, E. M.; McMurdie, H. F. Phase Diagrams for Ceramists; National Bureau of Standards.
(12) Wang, J.; Fu, P.; Wu, Y. Top-Seeded Growth and Morphology of $La_2CaB_{10}O_{19}$ Crystals. *J. Crystal Growth* **2002**, *235*, 5−7.
(13) Haumesser, P.-H.; Gaumé, R.; Benitez, J.-M.; Viana, B.; Ferrand, B.; Aka, G.; Vivien, D. Czochralski Growth of Six Yb-Doped Double Borate and Silicate Laser Materials. *J. Crystal Growth* **2001**, *233*, 233−242.

Received for review July 3, 2002. Accepted October 13, 2002.

JE025574T